Ni/SiO$_2$ and Ni/ZrO$_2$ catalysts for the steam reforming of ethanol

Ilenia Rossetti [a],[*], Cesare Biffi [a], Claudia L. Bianchi [a], Valentina Nichele [b], Michela Signoretto [b], Federica Menegazzo [b], Elisabetta Finocchio [c], Gianguido Ramis [c], Alessandro Di Michele [d]

[a] Dip. Chimica fisica ed Elettrochimica and INSTM Unit, Università degli Studi di Milano, via C. Golgi 19, I-20133 Milano, Italy
[b] Dip. di Scienze Molecolari e Nanosistemi and INSTM Unit, Università Ca' Foscari Venezia, Calle Larga S. Marta, 2137 Venezia, Italy
[c] Dip. di Ingegneria Chimica e di Processo "G. Bonino" and INSTM Unit, Università degli Studi di Genova, P.le Kennedy 1, I-16129 Genova, Italy
[d] Dip. di Fisica, Università degli Studi di Perugia, Via Pascoli, 06123 Perugia, Italy

ARTICLE INFO

ABSTRACT

SiO$_2$ and ZrO$_2$ supported Ni catalysts were prepared for use in the steam reforming of ethanol. The catalytic performances, in terms of both H$_2$ productivity and stability towards coking and sintering, were related to the physico-chemical properties of the catalysts.

The samples were prepared either by synthesis of the support by precipitation and subsequent impregnation with the active phase, or by direct synthesis through flame pyrolysis. The latter has been chosen because it leads to nanostructured oxides, often quenched in very disperse or metastable form, characterised by high thermal resistance, important for this high temperature application.

Many techniques have been used to assess the physico-chemical properties of the catalysts. The samples showed different textural, structural and morphological properties, as well as different reducibility and thermal resistance, depending on the preparation method and support. Therefore, besides evaluating the effect of catalyst formulation and preparation method on the catalytic performance, the influence of all such properties has been considered. The fundamental parameter governing the final catalyst properties was metal–support interaction. In particular, the stronger the latter parameter, the higher was metal dispersion, leading to small and stable Ni clusters. This influenced both activity and the resistance towards coking. Surface acidity was also taken into account considering the effect of the different nature of acid sites (silanols or Lewis a.s.) of both support and metal phase on catalyst deactivation. The best results were obtained with a 10 wt% Ni/SiO$_2$ sample, prepared by FP, when tested at 625 °C. H$_2$ productivity of 1.44 mol H$_2$/min kg$_{cat}$ was reached, corresponding to ca. 80% of the maximum value achievable under the selected conditions. This result was accompanied by the lowest CO/CO$_2$ ratio and 100% carbon balance without by-products in the outflowing gas.

© 2012 Elsevier B.V. All rights reserved.

1. Introduction

The steam reforming of biofuels, such as ethanol, represents a hot research topic of the last few years. Different metals have been proposed as active phase, e.g. Ni, Co and Cu, to consider just the less expensive non-noble metals, whereas the most used support is alumina, in case doped with alkali or lanthana to limit its acidity [1–5]. The most interesting results have been obtained with Co and Ni [6–8]. The latter seems very promising, though some drawbacks remain unsolved due to sintering and coking [6,9,10]. Indeed, very dispersed Ni particles tend to agglomerate during high temperature operations and in the presence of water vapour [11–14]. The loss of exposed active phase influences, activity, selectivity and coke formation, due to the easier formation of carbon filaments over big

Ni particles [15–17]. The possibility to operate at low temperature may be advantageous from this point of view, in order to limit Ni sintering. In addition, lower heat input would be required to sustain this endothermal reaction (the reaction is feasible above ca. 300 °C [18]). Nevertheless, thermodynamic investigations on coke formation routes indicate that coke accumulation may be more severe at 500 °C than at higher temperature [8,19]. The thermal resistance of the catalyst, as well as Ni interactions with the support, are then essential in determining the catalytic performance.

Of course activity and stability of the catalyst also depend on the nature of the support. The latter should activate both ethanol and water, it may ensure a suitable dispersion of the active phase, possibly stabilising it during the high temperature operation, but it is also responsible of coking if uncontrolled surface acidity is present. Indeed, strong acidity may lead to ethanol dehydration to ethylene, which oligomerises and polymerises. The dehydration activity is competitive with the dehydrogenation/decomposition route, which leads to acetate/glycolate surface intermediates, readily

---

decomposed into products ($CO/CO_2/H_2$) or reformable intermediates such as methane or acetaldehyde.

The aim of the work was the design and the characterisation of heterogeneous catalysts to be used for the steam reforming of ethanol. A series of Ni-based catalysts was prepared by using different synthetic procedures. The active phase was supported on SiO_2 (mesoporous SBA-15 or amorphous dense nanoparticles) and ZrO_2, chosen due to their different acidity and redox properties with respect to the most commonly used alumina. The samples were prepared by (i) synthesis by precipitation of the support, impregnation with the active phase and calcination at 800 °C to impart proper thermal resistance and (ii) by flame pyrolysis (FP), a special technique able to impart high temperature stability and to tune metal dispersion. Indeed, the FP technique allows the continuous and one-step synthesis of oxides, single or mixed, usually showing good phase purity, along with nanometer-size particles and hence very high surface area (up to 250 m^2/g). The latter parameter could help in improving low temperature performance in the present case. In addition, the high temperature of the flame in principle should also ensure thermal stability, provided that a solvent with sufficiently high combustion enthalpy is chosen [20,21].

The catalysts were characterised by different techniques, namely N_2 adsorption–desorption, temperature programmed reduction and oxidation (TPR–TPO), X-ray diffraction (XRD), atomic absorption (AA), X-ray photoelectron spectroscopy (XPS) infrared spectroscopy (FT-IR) and scanning or transmission electron microscopy (SEM–TEM). Activity testing data were then collected for the steam reforming of ethanol at different reaction temperatures.

2. Experimental

2.1. Catalyst preparation

2.1.1. Support synthesis

SBA-15 was synthesised as previously reported [22], in the presence of Pluronic 123 (P123, Aldrich) as structure directing agent. Silicon hydroxide was calcined at 800 °C for 6 h.

ZrO_2 was prepared by a conventional precipitation method [23] at a constant pH of 10.

2.1.2. Addition of the active phase

The active phase was added to each support by incipient wetness impregnation with an aqueous solution of the metallic precursor ($Ni(NO_3)_2 \cdot 6H_2O$, Sigma–Aldrich, purity ≥98.5%), in the proper concentration in order to obtain the desired Ni loading (10 wt%). The catalyst was dried overnight at 110 °C and then calcined at 800 °C for 4 h [24].

2.1.3. Catalysts synthesis by flame pyrolysis

A second set of samples was prepared in nanopowder form by means of a flame pyrolysis apparatus [25,26].

The SiO_2-supported sample was prepared by diluting TEOS (Fluka, pur. 99%) in xylene, with a 0.67 M final concentration referred to SiO_2, whereas the sample supported on ZrO_2 was produced from a Zr-acetylacetonate (Aldrich, 98%) solution. The active metal has been directly incorporated during the support synthesis. Ni was added to such mother solutions by dissolving Ni(II) acetate (Aldrich, pur. 98%) in propionic acid (Aldrich, pur. 97%) so to achieve a nominal 10 wt% metal loading with respect to the support oxide and a 1:1 (v/v) solution of the two solvents. The solutions were fed to the nozzle using a 50 ml glass syringe with a flow rate of 2.2 ml/min and a 1.5 bar pressure drop across the nozzle, cofed with 5 l/min of O_2.

Catalysts were named NiSi, or NiZr, where Si and Zr refer to SiO_2 and ZrO_2 carriers. The additional symbols L or F indicate the liquid phase synthesis of the support or preparation by FP, respectively.

2.2. Characterisation

In order to evaluate the actual metal concentration in the catalysts, atomic absorption spectroscopy measurements were carried out on a Perkin Elmer AAnalysis instrument after dissolution of the sample.

XRD patterns were collected on a Bruker D8 Advance diffractometer equipped with a Si(Li) solid state detector (SOL-X) and a sealed tube providing Cu Kα radiation. Phase recognition was possible by comparison with literature data [27].

Specific surface area and pores size distribution were evaluated through N_2 adsorption–desorption isotherms at −196 °C (Micromeritics, ASAP 2000 Analyser). Surface area was calculated on the basis of the BET equation [28], whereas the pores size distribution was determined by the BJH method [29], applied to the N_2 desorption branch of the isotherm. Prior to the analysis the sample was dried overnight at 110 °C and then outgassed in vacuum at the same temperature for 2 h.

XPS analysis has been carried out by means of a monochromatised SSI instrument.

TPR measurements were performed by placing the catalyst in a quartz reactor and heating by 10 °C/min from r.t. to 800 °C in a 5% H_2/Ar mixed gas stream flowing at 40 ml/min. TPO was carried out heating by 10 °C/min from r.t. to 800 °C in a 5 vol% O_2/He gaseous stream flowing at 40 ml/min. TPR–TPO–TPR cycles were performed on all the samples.

SEM images have been obtained using a Philips XL-30CP electron microscope and the surface and elemental composition of the catalysts was determined using energy dispersive X-ray measurements (EDX). The scanning electron microscope was equipped with a LaB$_6$ source and an EDAX/DX4 detector. The acceleration potential voltage was maintained between 15 keV and 20 keV and samples were metallised with gold.

TEM images have been obtained using a Philips 208 Transmission Electron Microscope. The samples were prepared by putting one drop of an ethanol dispersion of the catalysts on a copper grid pre-coated with a Formvar film and dried in air.

FT-IR spectra have been recorded under static conditions by a Nicolet Nexus Fourier transform instrument, using conventional IR cells connected to a gas manipulation apparatus. Pressed disks of pure catalyst and support powders (∼20 mg) were thermally pretreated in the IR cell by heating in vacuum at 500 °C. For reducing the samples, after this pretreatment, they were heated in pure H_2 at 500 °C (600 Torr, two cycles, 30 min each) followed by an evacuation step at the same temperature. CO adsorption experiments have been performed at liquid nitrogen temperature and following outgassing upon warming.

Pivalonitrile (PN) adsorption experiments have been performed over the reduced samples at room temperature and following outgassing at increasing temperatures.

2.3. Ethanol steam reforming (ESR)

Activity tests were performed by means of a micropilot plant constituted by an Incoloy 800 continuous downflow reactor (*i.d.* 0.9 cm, length 40 cm), heated by an electric oven. The reactor temperature was controlled by an Eurotherm 3204 TIC. The reactor may be fed both with liquid and gaseous reactants and at the reactor outlet there is a trap for the collection of possible liquid products and a gas sampling point.

Table 1
Main physical–chemical properties of the samples prepared.

Sample	Preparation method	Ni loading (wt%)[a]	SSA (m²/g)[b]	Mean pore size (nm)	Crystal size (nm)[c]
NiSiL	SBA-15 calcined at 800 °C	8.9	309 (IV-type isotherm)	6.0 (H1 hysteresis)	21 (20–30)
NiZrL	ZrO₂ prepared by precipitation with NH₄OH, calcined at 800 °C	8.8	43 (IV-type isotherm)	18.7 (H3 hysteresis)	18 (ca. 20)
NiSiF	Flame pyrolysis	9.6	211	13.1	18 (20–30)
NiZrF	Flame pyrolysis	8.8	83	13.1	8 (10–15)

[a] From atomic absorption analysis.
[b] SSA: specific surface area, from BET model.
[c] Crystal size determined by the Scherrer equation and TEM between parentheses.

The catalysts were pressed, ground and sieved into 0.15–0.25 mm particles and ca. 0.5 g were loaded into the reactor after dilution 1:3 (v/v) with SiC of the same particle size.

Catalyst activation was accomplished by feeding 50 cm³/min of a 20 vol% H_2/N_2 gas mixture, while heating by 10 °C/min up to 800 °C, then kept for 1 h. During activity testing 0.017 cm³/min of a 3:1 (mol/mol) $H_2O:CH_3CH_2OH$ liquid mixture were fed to the reactor by means of a Hitachi, mod. L7100, HPLC pump, added with 56 cm³/min of N_2, used as internal standard, and 174 cm³/min of He. Such dilution of the feed stream was calibrated so to keep the reactants mixture in the vapour phase even at zero conversion at the reactor outlet. The high temperature (HT) activity tests were carried out at atmospheric pressure, GHSV = 2500 h^{-1} (referred to the ethanol + water gaseous mixture) at 500, 625 and 750 °C.

The analysis of the out-flowing gas was carried out by a gas chromatograph (Agilent, mod. 7980) equipped with two columns connected in series (MS and Poraplot Q) with a thermal conductivity detector (TCD), properly calibrated for the detection of ethanol, acetaldehyde, acetic acid, water, ethylene, CO, CO_2, H_2. Material balance on C-containing products was checked to quantify coke deposition.

Repeated analyses of the effluent gas were carried out every hour and the whole duration of every test at each temperature was ca. 8 h.

The raw data, expressed as mol/min of each species outflowing from the reactor, have been elaborated as follows.

Products distribution [7]: Y_i = mol i/Σ(mol i)
C balance: $100 - (((mol\ CH_3CH_2OH * 2)_{in} - \Sigma (mol\ C_i * \chi_i)_{out})/(mol\ CH_3CH_2OH * 2)_{in}) * 100$
Conversion: $X_i = (mol\ i_{in} - mol\ i_{out})/mol\ i_{in}$ $i = H_2O, CH_3CH_2OH$
Selectivity: $S_i = (mol\ i/\nu_i)/(mol\ ethanol_{in} - mol\ ethanol_{out})$
H_2 yield: Yield $= X_{ethanol} * S_{H_2} = mol\ H_2/\nu_{H_2} * mol\ ethanol_{in}$
H_2 productivity: mol H_2 out/min kg$_{cat}$

where i = products detected, dry basis; χ_i = number of C atoms in the ith molecule; ν_i = stoichiometric coefficient of species i in the ESR reaction.

3. Results and discussion

3.1. Textural, structural and morphological characterisation

The textural properties of the samples prepared and the actual concentration of Ni are reported in Table 1.

The FP prepared samples were characterised by different surface areas depending on the support. According to [20,21], this is tightly related to the decomposition mechanism of the oxide precursor in the flame and to the type of solvent used. Sample NiSiL exhibited the highest surface area and retained its mesoporous structure in spite of the high calcination temperature. By contrast, catalyst NiZrL did not prove very thermally resistant, since its surface area was the lowest.

The results of surface analysis (XPS) are summarised in Table 2, as relative atomic percentage. The Ni fraction exposed on the support surface was higher for samples obtained by FP. This is reasonable considering the direct incorporation of the metallic active phase during the synthesis of the catalyst and confirmed that the flash calcination characteristic of the technique did not allowed significant phase segregation. By contrast impregnation led to lower Ni dispersion and consequently to a lower Ni exposure over the surface. Likely, both silica supports exhibited a sufficiently high surface area to adequately disperse the selected loading of the active phase. By contrast when surface area was lower, as in the case of the zirconia support, higher metal aggregation was achieved by impregnation (i.e. lower surface exposure) than when Ni was directly incorporated into the support during the FP synthesis. Therefore, the advantage of the latter technique is mainly evident when surface area is not very high, as in the case of NiZrF, whose fraction of Ni exposed was the highest. Similar considerations have been extensively discussed for different catalytic systems prepared by FP [30–33]. Examples of XPS spectra in the Ni 2p region are reported in Fig. 1. As for the oxidation state, the highest has been always found for Ni in the fresh samples.

The TPR technique was employed to identify possibly different metal species present in the catalysts according to their reduction temperature. Moreover, this technique allows to estimate the strength of interaction between the active phase and the support. It is well-known that such interaction increases with calcination temperature and this may be of outmost importance in order to stabilise Ni particles and to achieve satisfactory catalytic activity, as introduced above. Furthermore, TPR–TPO–TPR cycles were carried out to check the reversibility of Ni reduction. In principle, the preparation procedure, mainly flame pyrolysis, may induce at least a partial incorporation of Ni into the support, possibly leading to a mixed oxide phase. It may be supposed that some reconstruction of the oxide may occur during metal reduction. Moreover, Ni that is initially well dispersed in the support, as discussed for the XPS data (vide supra), after a first reduction process mimicking catalyst activation, may arrange in bigger clusters, likely characterised by a different reducibility. Therefore, the second TPR run may help

Table 2
Surface analysis by XPS. Data reported as atomic percent or ratio.

Sample	Surface Ni	Surface Si, Zr	Ni/(Si,Zr) ratio
NiSiL	0.8	33.5	0.02
NiZrL	1.2	14.4	0.083
NiSiF	1.4	30.3	0.05
NiZrF	2.2	13.3	0.16

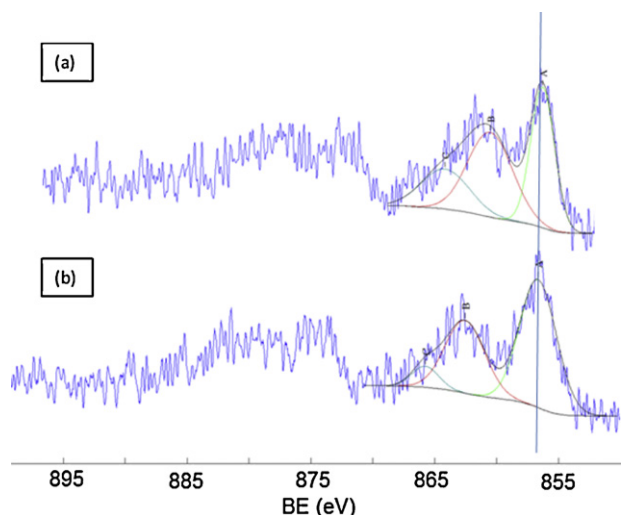**Fig. 1.** XPS spectra in the Ni 2p region. Peak A: $Ni_{2p3/2}$, peaks B and C: shake-up. (a) NiSiL and (b) NiSiF.

to elucidate the features of surface Ni particles in the activated samples. The results are reported in Fig. 2.

TPR measurements show that all the catalysts were completely reduced in H_2 below 750 °C. Regardless of the nature of the support, the presence of various peaks was observed that can be ascribed to NiO species differently interacting with the oxide support. In particular the peaks at lower temperature are related to NiO weakly interacting with the support, whereas the peaks at high temperature indicate a strong metal/support interaction [34,35]. In the first TPR of the as prepared FP samples the reduction peaks appear at lower temperatures with respect to impregnated catalysts,

denoting weaker interactions between Ni and the support. Moreover, this could indicate a higher availability of surface Ni, as confirmed by XPS data (*vide supra*). In particular, the first TPR of NiSiF catalyst revealed an almost featureless broad peak centred around 450 °C, attributed to NiO reduction. The metal may be oxidised back at *ca.* 300 °C and the second reduction (Fig. 2) resulted almost equivalent to the fresh sample, indicating on one hand a quite perfectly reversible reduction/oxidation cycle, on the other hand a very broad heterogeneity of Ni oxide sites, remaining even after activation of the sample. Only a slight increase of the reduction temperature was observed, indicating that a bit stronger interaction between Ni and the support has been achieved upon activation without significant rearrangement or sintering of the active phase.

The TPR profile of the NiSiL catalyst evidenced different reduction zones: the first peak is well-defined, while the second peak appears as a broad shoulder in the temperature range between 420 and 700 °C, where at least two overlapping features are evident. This means that a fraction of NiO particles is characterised by weak interactions with the support, while a greater portion of them strongly interacts with silica [36,37]. After oxidation, occurring at 400–550 °C, the second TPR run evidenced the presence of more reducible species, likely due to metal sintering, which leads to bigger Ni particles, characterised by higher reducibility [38].

For sample NiZrL the higher temperature peak (with its maximum at 655 °C) can be assigned to NiO particles strongly interacting with the ZrO_2 surface, while the peak at lower temperature (shoulder at about 450 °C) is due to NiO species weakly interacting with the support [35,39]. Also for the FP-prepared NiZrF sample (Fig. 2), two NiO species may be found, though this sample revealed in general much more reducible than NiZrL.

The subsequent TPO showed that Ni oxidation occurred at *ca.* 350 °C for sample NiZrL and at *ca.* 240 °C for catalyst NiZrF. The last TPR run evidenced that the distinction between different Ni
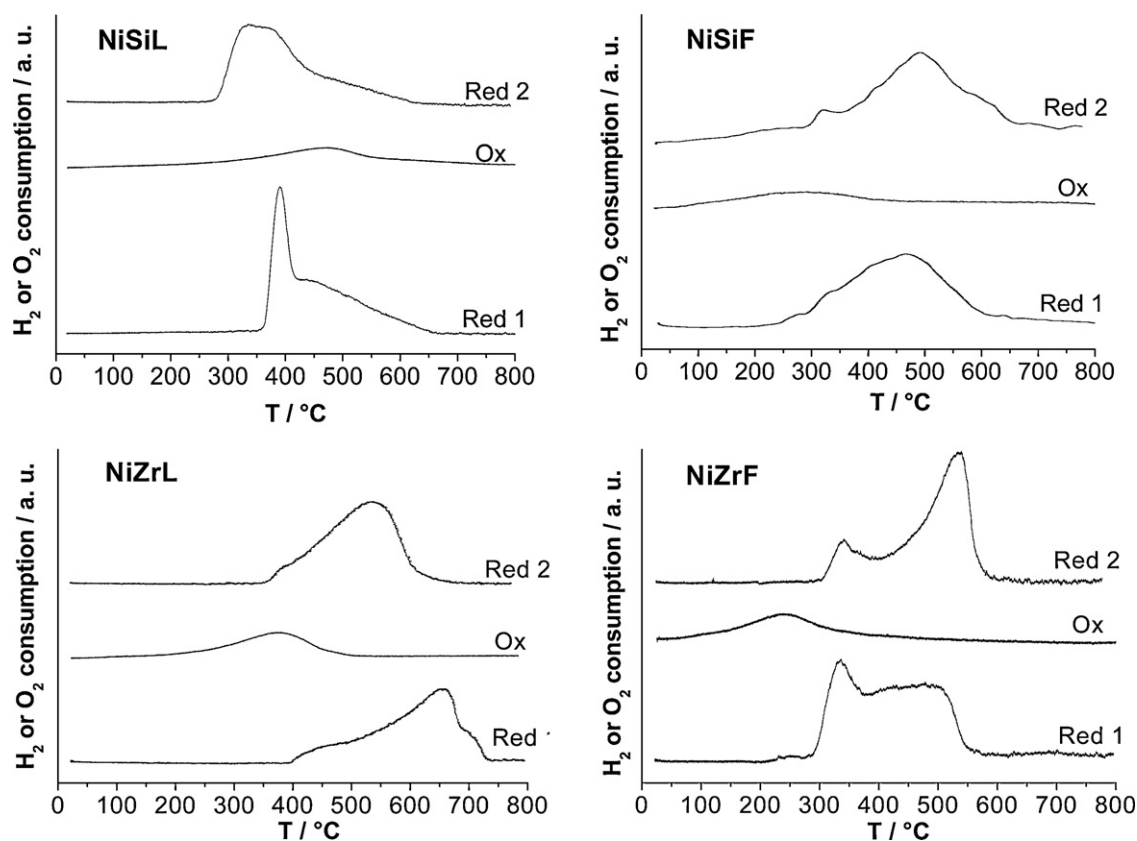

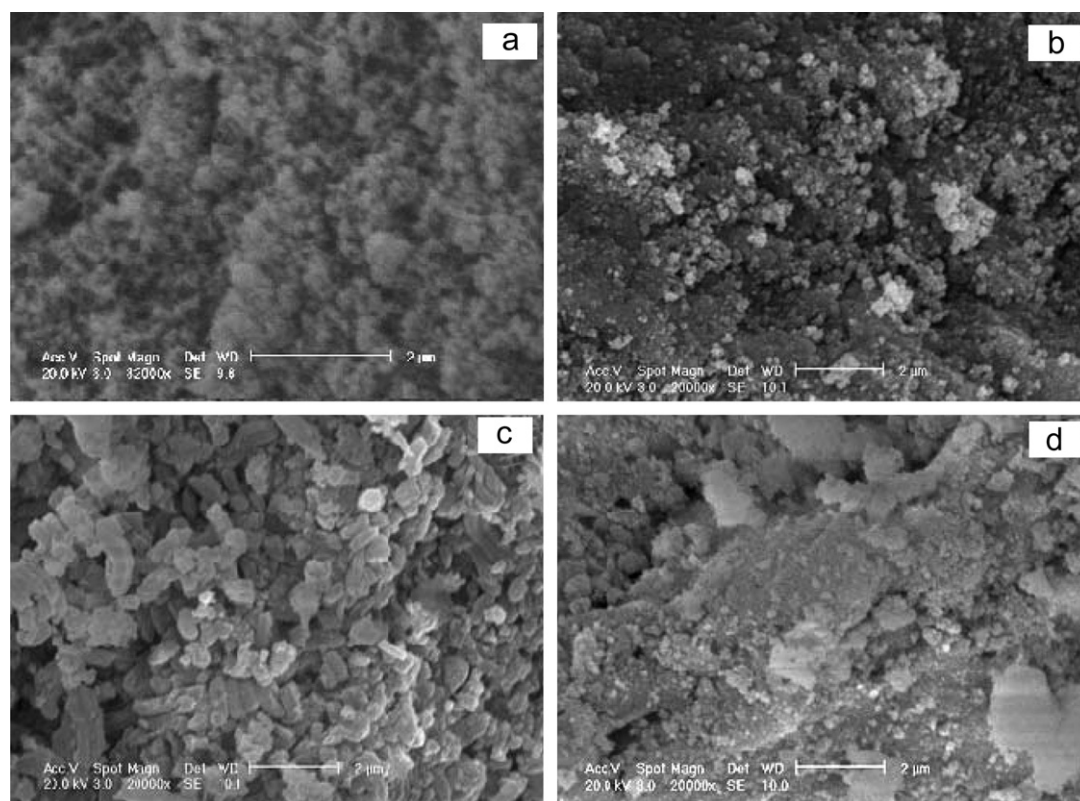**Fig. 2.** TPR–TPO–TPR analysis of the prepared samples.

Fig. 3. SEM micrographs of (a) NiSiF, (b) NiZrF, (c) NiSiL, and (d) NiZrL. Marker size 2 μm.
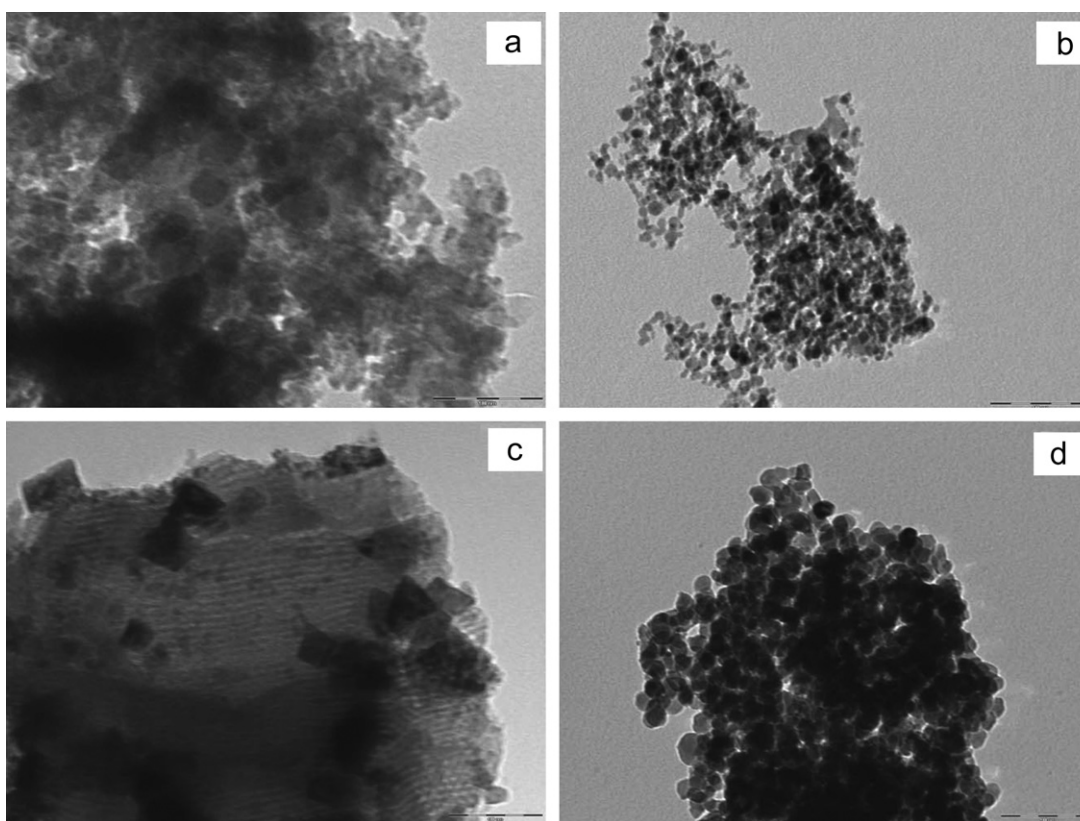

Fig. 4. TEM micrographs of (a) NiSiF, (b) NiZrF, (c) NiSiL, and (d) NiZrL. Marker size 100 nm.

species was retained, especially for sample NiZrF, for which the second peak became more intense and shifted towards higher temperature, testifying the formation of stronger Ni-support interactions after the first treatment. Contrarily, sample NiZrL became more reducible after the first redox cycle, likely due to metal sintering, as already observed with NiSiL [38].

In general, NiO species impregnated over supports prepared by precipitation seem less reducible when fresh, than those synthesised by FP. Likely, in the latter Ni is quenched into the support matrix in metastable form [30–33] and rearranges after the first activation. The Ni clusters thus formed result very dispersed and are characterised by lower reducibility, *i.e.* by a stronger metal–support interaction, with respect to Ni deposited by impregnation, which more easily sinters after activation.

XRD analyses after reduction were performed in order to identify the different phases present in the samples. Ni crystal size was calculated from the Scherrer equation (Table 1).

The XRD pattern of NiSiL sample revealed the mesoporous structure of the support and this feature was preserved in spite of the high calcination temperature. The diffraction peaks obtained for the NiZrL sample can be mainly assigned to the tetragonal structure of ZrO_2, coupled with a 19% of monoclinic phase. Peak broadening was observed in the XRD pattern of sample NiZrF, due to the nanometer particle size, while silica prepared by FP was amorphous.

The Ni crystal size was a bit higher for NiSiL than for NiSiF (Table 1) in spite of its higher surface area. Ni dispersion sensibly decreased when passing from SiO_2 to ZrO_2, as expected due the higher surface area of the former sample.

In general, we may conclude that Ni dispersion was dependent on both the surface area of the support and the metal/support interaction.

Complementary structural information may be drawn from the skeletal FT-IR spectra. Both the Ni/SiO_2 samples showed the typical features of silica-based materials at $1100\,cm^{-1}$ (shoulder at $1250\,cm^{-1}$), 800 and $450\,cm^{-1}$ [40]. In addition, the spectra of the zirconia based samples were consistent with the presence of monoclinic ZrO_2 (band at $745\,cm^{-1}$) together with the most abundant tetragonal phase, whose peaks are overlapped with monoclinic phase in the low frequency region.

SEM micrographs of the FP-prepared catalysts revealed they were constituted by a rather uniform array of nanoparticles, whereas bigger particle size was observed for NiSiL and NiZrL samples (Fig. 3). EDX analysis also confirmed the Ni loading with respect to atomic absorption and repeated analyses in different zones demonstrated a uniform distribution of the active phase. The latter conclusion has been also supported by several maps.

A more detailed view on sample morphology and particle size was obtained by TEM analysis (Fig. 4), which showed lower Ni crystal size for NiZrF than for NiSiF (Table 1), in accordance with estimations from XRD analysis.

The NiSiL sample was constituted by very big crystals, where the single particle domains were scarcely recognised. The SBA-15 channel structure was evident (Fig. 4c), as well as the presence of Ni particles with markedly different size, from few nm to 20–30 nm, in accordance with the average Ni crystal size calculated from XRD data (Table 1). Finally, sample NiZrL showed a very uniform and nanometric particle size (*ca.* 20–30 nm), with similar size of the Ni particles. Likely, Ni uniformly and rather completely covered the support due to its low surface area.

3.2. FT-IR analysis

The surface spectra (not reported) of the activated NiSiF catalyst show the typical features of silica at $3745\,cm^{-1}$ (OH stretching mode), 2000–$1800\,cm^{-1}$ (Si—O overtones) and the cut off near $1300\,cm^{-1}$. Reduction with hydrogen of the metal phase did not
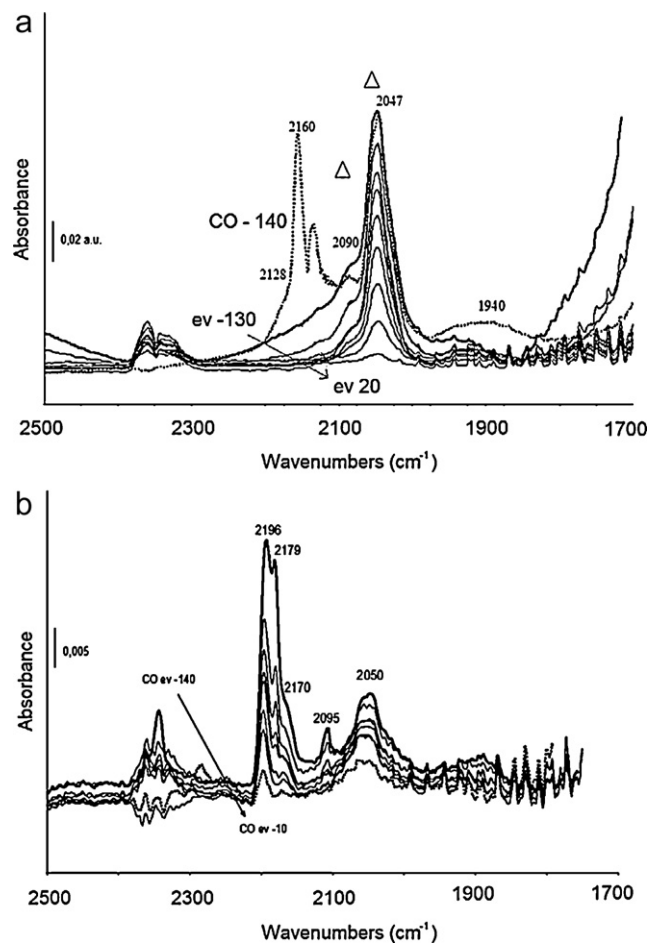

Fig. 5. FT-IR subtraction spectra of surface species arising from CO adsorption over NiSiF reduced catalyst at liquid nitrogen temperature and upon warming to r.t. (a) Hydrogen-reduced catalyst and (b) outgassed catalyst. The activated surface has been subtracted.

lead to any significant change of the spectrum. Possibly a weakening of the silanols band and a correspondingly increasing intensity of the H-bound hydroxyl groups could be the result of water vapour formed during reduction.

In the spectra recorded upon CO adsorption over the reduced sample (Fig. 5a, dotted line), the strong bands at 2160, 2140 and $2100\,cm^{-1}$ were due to CO interacting with OH groups and weakly physisorbed and they disappeared almost completely after outgassing at liquid nitrogen temperature. The intense and asymmetric band at $2047\,cm^{-1}$ together with the weak band centred at $1940\,cm^{-1}$ were due to terminal carbonyls and bridging carbonyls, respectively. For high loading and highly reduced Ni catalysts quite broad bands were usually observed upon CO adsorption at 2080–$2020\,cm^{-1}$ and at 1930–$1870\,cm^{-1}$, typically assigned to terminal and bridging carbonyls on extended Ni metal particles [41–44].

The several weak components detected above $2000\,cm^{-1}$ suggest the formation of Ni^+ polycarbonyl species (Fig. 5a). In particular, in the region 2000–$2100\,cm^{-1}$ the weak bands at 2130 and $2090\,cm^{-1}$ were assigned to $Ni^+(CO)_2$, while shoulders at 2038 and $2070\,cm^{-1}$, with similar relative intensities, could be due to Ni^0 polycarbonyls, such as $Ni(CO)_3$, likely frozen precursors of the formation of $Ni(CO)_4$. This may be seen as indication of the existence of atomically dispersed zerovalent nickel [45,46]. The relative intensities of the features here reported indicate that nickel was mainly present as metal, moreover, the detection of bridging species was
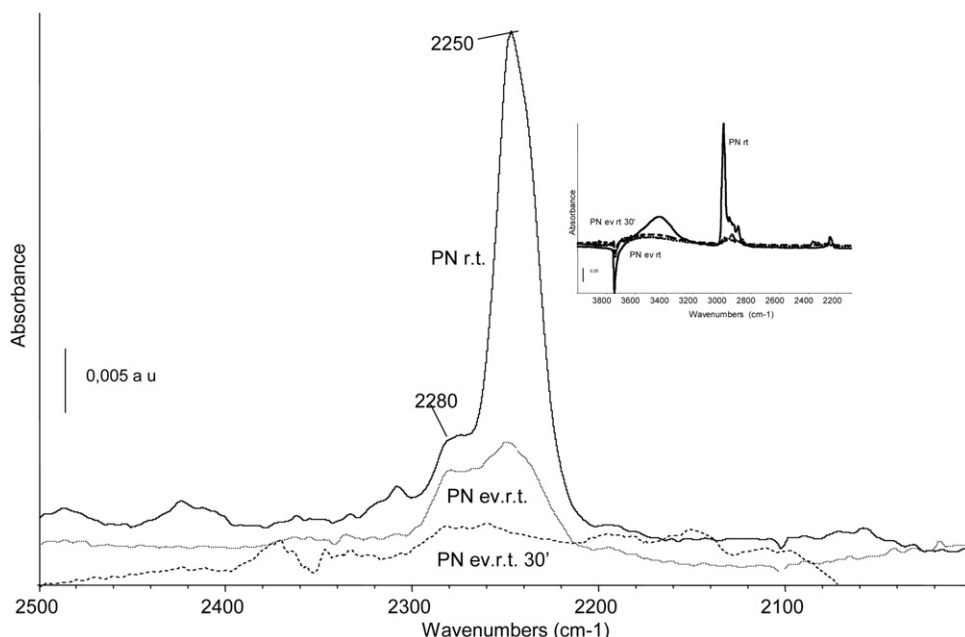
Fig. 6. FT-IR subtraction spectra of surface species arising from PN adsorption over reduced catalyst NiSiF at r.t. and after prolonged outgassing. The activated surface has been subtracted. Inset: OH stretching region.

an indication of large particles formation, which can be related to a high Ni reducibility.

CO adsorption at low temperature has been also performed over the outgassed catalyst, *i.e.* following a thermal treatment in vacuum and not in hydrogen (Fig. 5b), in order to confirm the previous assignment to ionic Ni species. This pretreatment resulted in the detection of three sharp bands at 2196, 2179, 2170 cm^{-1}, thus in the spectral range typical of CO coordinated over Ni^{2+} and Ni^{+} ions species, as expected. In particular, the split of the high frequency band was an evidence of at least two kinds of Ni^{2+} ions. However, traces of Ni metal particles, likely formed during the preparation/pretreatment step could be detected, characterised by weak bands due to terminal carbonyls below 2100 cm^{-1}. This effect also confirmed the high Ni reducibility for this sample.

PN adsorption over the reduced catalyst led to the spectra reported in Fig. 6. Two bands were detected in the CN stretching region: at 2250 cm^{-1}, strong, and 2280 cm^{-1}, by far weaker. The former disappeared already following outgassing at room temperature. The position and behaviour of these bands allowed their attribution to PN interacting with silanol groups (H-bound species, weakly held) and to PN interacting with medium Lewis acidic centres, respectively (possibly the metal phase).

In the FT-IR spectra (not reported) of catalyst NiSiL no isolated free silanol bands could be detected following the reduction treatment, but only a broad and strong signal around 3700 cm^{-1}, tailing towards lower frequencies, due to an increased formation of H-bonds amongst disordered hydroxy groups. Likely, impregnation
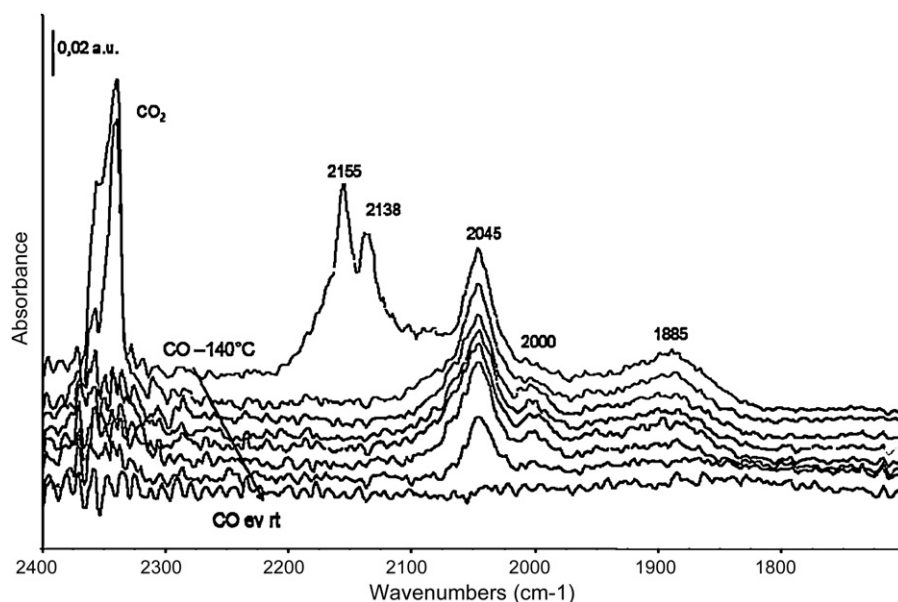

Fig. 7. FT-IR subtraction spectra of surface species arising from CO adsorption over NiSiL reduced catalyst at liquid nitrogen temperature and after warming to r.t. The activated surface has been subtracted.
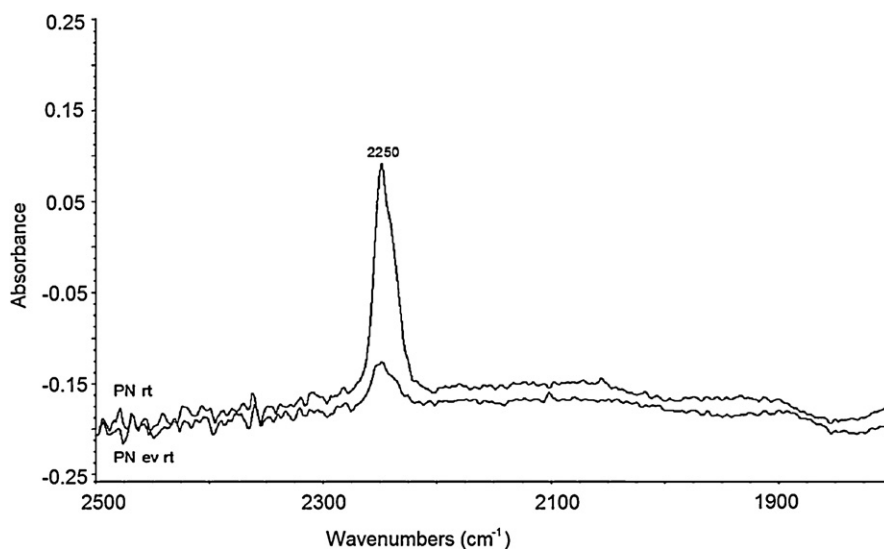
Fig. 8. FT-IR subtraction spectra of surface species arising from PN adsorption over NiSiL reduced catalyst at r.t. and following outgassing at r.t. The activated surface has been subtracted.

of the support with Ni nitrate solution affects hydroxyl groups, working as surface germination sites during the impregnation step. The following thermal and/or reduction treatments do not restore the support initial hydroxyl groups, and this effect can be taken as an evidence of a significant metal–silica interaction. In the spectra recorded following CO adsorption (Fig. 7), strong bands at 2155 and 2138 cm^{-1}, also in this case tailing towards lower frequencies, were attributed to CO interacting with OH groups and weakly physisorbed, completely disappearing following outgassing. The strong band at 2045 cm^{-1} was assigned to terminal carbonyls over Ni metal particles and the weak absorption at 1885 cm^{-1} was ascribed to bridging carbonyls on extended Ni metal particles. Following outgassing upon warming, another component appeared at 2000 cm^{-1}, thus in the frequency range characterising carbonyls over Ni metal particles possibly exposing different facets. The formation of polycarbonyls over ionic and metallic Ni clusters (bands at 2130–2090 cm^{-1}) was strongly limited, if any. On the other side,

the formation of CO_2 (bands around 2350 cm^{-1}) during the low temperature CO adsorption can be taken as an indirect evidence of some residual Ni ions species exposed at the catalysts surface even after reduction treatments and able to oxidise CO.

PN adsorption (Fig. 8) revealed, as expected, only H-bound species, characterised by one band at 2250 cm^{-1}, readily disappearing following outgassing. The comparison with spectra reported in Fig. 6 points out that no Lewis acidity has been induced in this sample following Ni impregnation, contrarily to sample FP.

Spectra of CO adsorption over the NiZrF catalyst are reported in Fig. 9. The very low quality of the spectra is due to the very low (near 1%) transmittance of the sample in the CO spectral region, likely due to light scattering for particle size reasons or to the presence of reduced metal. However, some bands can be detected. In particular near 2075 cm^{-1} an absorption is evident due to CO linearly coordinated over Ni^0. Moreover, CO adsorption over Zr^{4+} Lewis a.s. was responsible of the band near 2175 cm^{-1}. In these conditions,

Fig. 9. FT-IR subtraction spectra of surface species arising from CO adsorption over NiZrF reduced catalyst, at liquid nitrogen temperature and after warming. The activated surface has been subtracted. Spectra recorded from −140 to −80 °C, with step 15 °C.
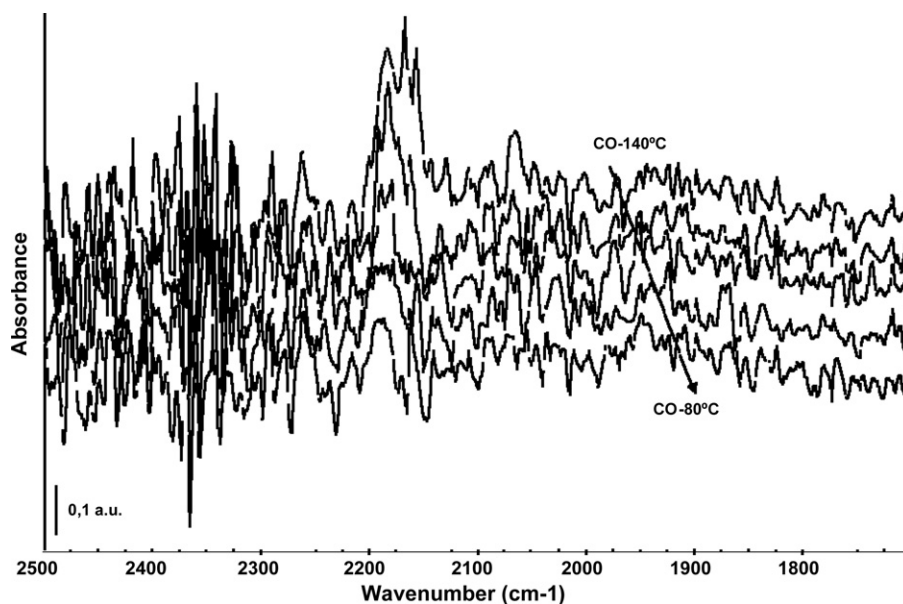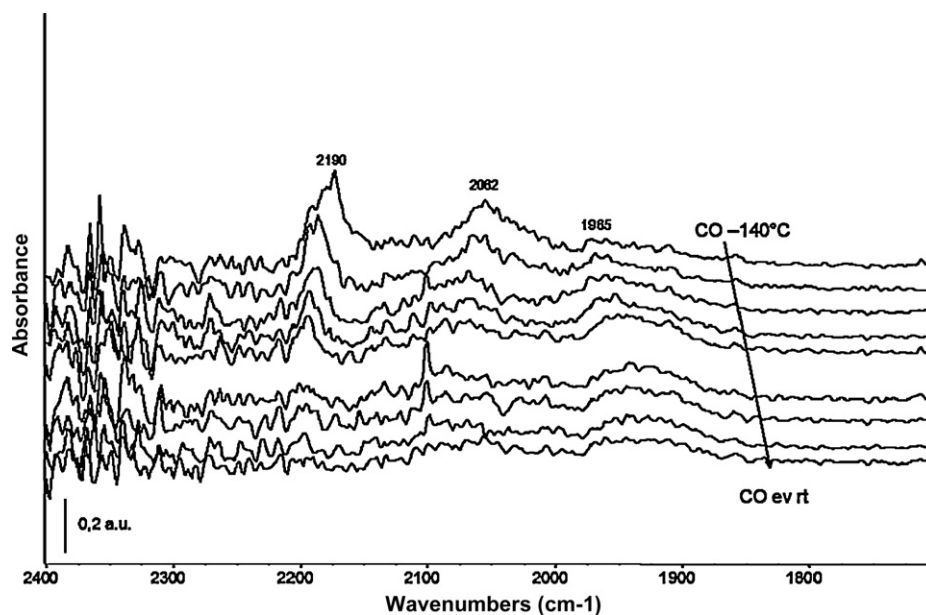
Fig. 10. FT-IR subtraction spectra of surface species arising from CO adsorption over NiZrL reduced catalyst at liquid nitrogen temperature and after warming to r.t. The activated surface has been subtracted.

PN adsorption (not reported) does not provide further indications on the surface acidity.

After CO adsorption over NiZrL, three main bands could be detected at 2190, 2062 and 1969 cm^{-1}, although very weak and noisy (Fig. 10). The former was due to carbonyl over exposed Zr ions. This band decreased in intensity following outgassing and shifted to higher frequencies, in agreement with the proposed assignment. Bands below 2100 cm^{-1} were assigned to CO on-top and bridging over Ni metal particles.

PN adsorption (Fig. 11) over the same catalyst led to the detection of a weak and broad band at 2275 cm^{-1}, due to nitrile coordinated over exposed Zr^{4+} acidic sites, in agreement with data from CO adsorption.

CO and PN adsorption, studied by FT-IR spectroscopy over the reported Ni-based catalysts, allowed the following concluding remarks. Medium Lewis acidity due to exposed support ions was detected over the zirconia based catalysts, due to surface Zr ions, whereas over silica supported catalysts only in the NiSiF catalyst, Lewis acidity was induced by the metal phase itself.

As for the exposed metal phase, over the hydrogen-reduced samples (500 °C), for both FP and impregnated silica based catalysts a quite heterogeneous population of Ni species was detected: residual Ni$^+$ ions, Ni clusters and larger metallic Ni particles, characterized by different spectroscopic features. Metal Ni aggregates are predominant, in form of structured and large particles allowing the detection of CO bridging species, in agreement with results from XRD and TEM (Table 1). Moreover, the analysis of OH stretching region suggests that, for the fresh samples, Ni deposition leads to NiO$_x$ species strongly interacting with the support especially for the impregnated samples, thus confirming TPR results. Therefore, all the characterisation data evidenced marked differences of the samples, depending on catalyst formulation and the preparation procedure. As it will be described in the next section, only some properties proved significant to explain differences in catalytic activity and resistance.

3.3. Catalytic activity for the ESR

The tests for ethanol SR have been carried out on each catalyst and the results have been summarised in Table 3. If not else

specified the data represent the average performance over the last 4–8 h-on-stream, i.e. when each catalyst reached a stable steady state condition. Anyway, the qualitative inspection of the full data set at every temperature allowed to determine the stability of the sample. Possible by-products are described in the text. Reporting average values in the same table may be misleading, since their evolution with time-on-stream is often the most informative datum.

3.3.1. Blank tests

A blank test was carried out on the reactor filled with quartz beads and SiC, but without any catalyst. At 750 °C ethanol conversion was rather high, indeed after starting values higher than 80% it attested on *ca.* 50%, due to thermal activation of the substrate, in accordance with literature data [47]. However, the main products at the reactor outlet were acetaldehyde ($S_{CH_3CHO} = 60\%$) and ethylene ($S_{CH_2CH_2} = 20\%$). Poor ethanol decomposition to CO, no CH$_4$ or CO$_2$ were achieved and no evidence of coke deposition was observed due to 100% C balance. Therefore, thermal activation at 750 °C was sufficient to promote both the dehydrogenation (mostly) and dehydration reactions, but no further conversion of the products could be obtained. By lowering the reaction temperature to 500 °C *ca.* 15% ethanol conversion was still observed, but with C balance closing to 91% only, due to coke deposition on the reactor filling material. In this case acetaldehyde was the main product and no evidence of ethylene was found at the reactor outlet, likely due to its full polymerisation to form coke.

It should be taken into account that the high Ni content of the Incoloy reactor here adopted may in principle affect activity. This has been of course included in the blank test evaluation. However, when looking at the results of such preliminary runs, one may notice that ethanol dehydration and dehydrogenation predominantly occurred. This would suggest that the major concern would be acid sites (possibly filling quartz) than metal ones. This conclusion is also supported by similar results of a blank run carried out on a different apparatus equipped with a quartz reactor [47].

3.3.2. Catalyst NiZrL

Sample NiZrL tested at 750 and 625 °C, led to complete ethanol conversion without undesired by-products (methane and acetaldehyde) sometimes found with other samples even at the
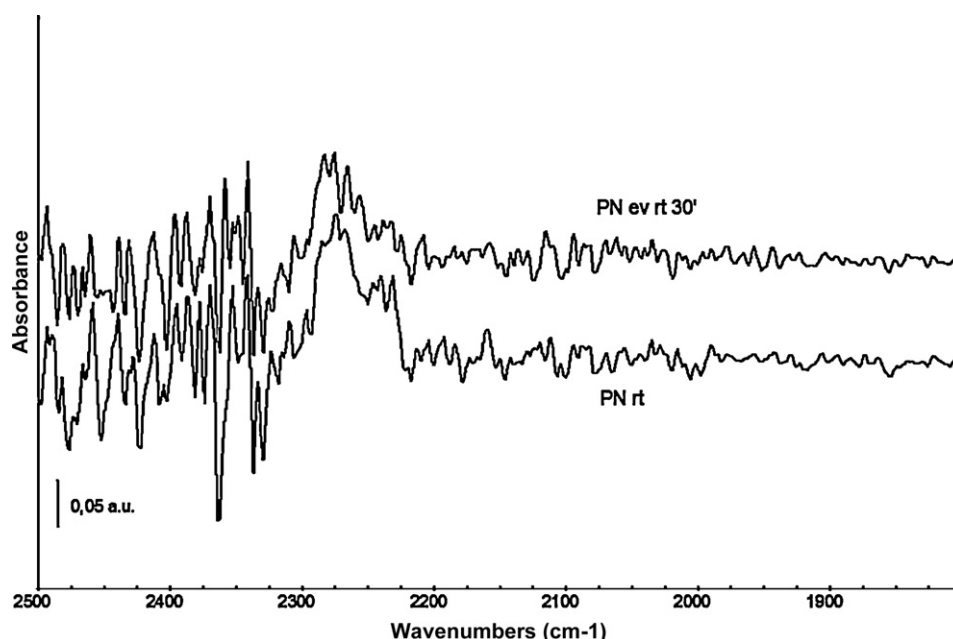
Fig. 11. FT-IR subtraction spectra of surface species arising from PN adsorption over NiZrL reduced catalyst at r.t. and following outgassing at r.t. The activated surface has been subtracted.

Table 3
Results of activity tests for the steam reforming of ethanol. Average values over 4–8 h-on-stream. Maximum H_2 productivity = 1.83 mol/min kg_{cat}. Productivity for blank tests expressed as mol_{H_2}/min. The evolution of possible by-products with time-on-stream is described along the text.

	Blank test	NiSiL	NiZrL	NiSiF	NiZrF
500 °C					
CO/CO_2	0.00 ± 0.00	0.52 ± 0.02	0.59 ± 0.08	0.58 ± 0.02	0.73 ± 0.02
C balance (%)	91 ± 2	74.6 ± 0.6	86.8 ± 1.5	88+2	94.3 ± 1.2
Conv. EtOH	0.13 ± 0.05	1.00 ± 0.00	1.00 ± 0.00	0.80 ± 0.02	0.60 ± 0.03
H_2 productivity (mol/min kg_{cat})	0.00 ± 0.00	1.03 ± 0.02	1.19 ± 0.09	0.889 ± 0.014	0.56 ± 0.02
625 °C					
CO/CO_2	–	1.20 ± 0.08	1.42 ± 0.09	1.1 ± 0.2	1.33 ± 0.16
C balance (%)	–	99.0 ± 1.1	90 ± 2	102 ± 2	101 ± 2
Conv. EtOH	–	1.00 ± 0.00	1.00 ± 0.00	1.00 ± 0.0	1.00 ± 0.0
H_2 productivity (mol/min kg_{cat})	–	1.369 ± 0.011	1.45 ± 0.05	1.442 ± 0.014	1.34 ± 0.13
750 °C					
CO/CO_2	Only CO	1.72 ± 0.13	2.32 ± 0.18	1.72 ± 0.01	2.18 ± 0.09
C balance (%)	103 ± 3	102 ± 3	96.7 ± 1.5	99.2 ± 1.3	101.8 ± 1.9
Conv. EtOH	0.54 ± 0.04	1.00 ± 0.00	1.00 ± 0.00	1.00 ± 0.0	1.00 ± 0.0
H_2 productivity (mol/min kg_{cat})	0.061 ± 0.006	1.39 ± 0.03	1.36 ± 0.04	1.39 ± 0.03	1.24 ± 0.05

highest temperatures (*vide infra*). The carbon balance was satisfactory at 750 °C, though not optimal at 625 °C. By further lowering the reaction temperature to 500 °C carbon balance decreased, in accordance with thermodynamic previsions [48] and competitive kinetics between C accumulation and gasification [8]. Nevertheless, ethanol conversion remained complete and the catalyst behaviour appeared stable (Fig. 12), indicating that coking was extensive, but it was not severely deactivating the active phase. Some by products were observed, such as methane (selectivity *ca.* 11%), as expected due to incomplete methane reforming at low temperature [19,47,49]. Some ethylene outflowed after 5 h-on-stream, while acetaldehyde was never observed.

Similar or slightly lower CH_4 selectivity has been reported for Ni/ZnO–ZrO₂ [50] and Ni/La₂O₃–ZrO₂ catalysts (*ca.* 3–4 mol% at 500 °C in the products distribution, though *ca.* 0.1–1.5 mol% methane was still present at 650 °C) [51]. Yttria stabilised zirconia also proved an interesting support for Ni, showing full ethanol conversion even at 400 °C, though accompanied by very high selectivity to CH_4 (30–40%) at such temperature, so unacceptably lowering hydrogen yield [18].

3.3.3. Catalyst NiSiL

Similar comments may be drawn for sample NiSiL, with the main difference that water conversion was very low (the same conclusion apparently applies to both the silica based samples here investigated). Different water utilisation has been already reported
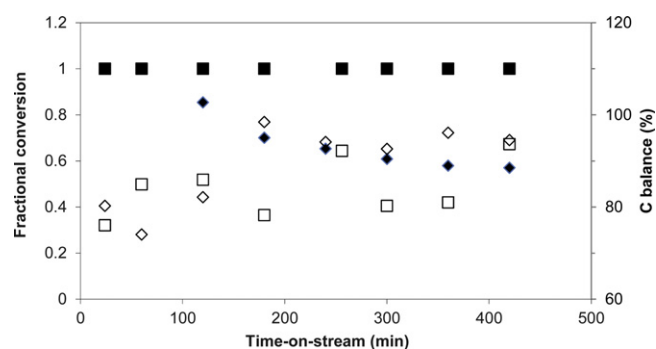

Fig. 12. Ethanol conversion (full symbols) and C balance *vs.* time-on-stream for samples NiZrL (square) and NiZrF (diamonds). Reaction temperature 500 °C.

Fig. 13. Products distribution during activity testing of sample NiSiL. Reaction temperature 500 °C.

Fig. 14. Ethanol conversion (full symbols) and C balance vs. time-on-stream for samples NiSiL (square) and NiSiF (diamonds). Reaction temperature 500 °C.
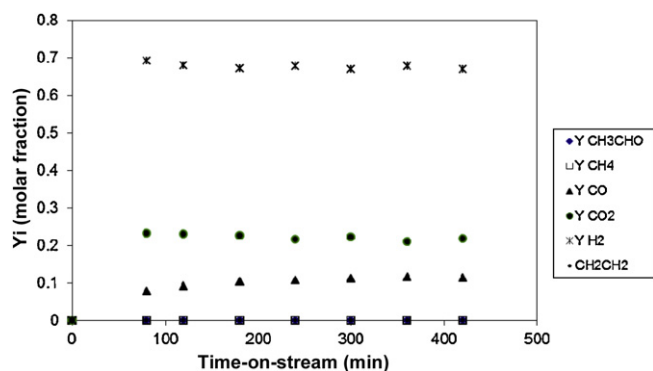
in the literature as a function of the support nature and reaction conditions [8,52] and often related to the dehydration reaction [9,53]. The latter may not always induce catalyst deactivation by coking, provided that the catalyst is also able to promote the fast reforming of the olefins formed.

At 625 °C water conversion slightly increased with respect to 750 °C, due to a higher contribution of the water gas shift (WGS) reaction, as confirmed by a lower CO/CO_2 ratio. At the lowest reaction temperature this sample gave rise to complete ethanol conversion without by-products (Fig. 13), but H_2 productivity was lower than for the Zr-supported catalyst and the C balance was much worse. Likely, this sample was very active for ethanol dehydration and it was able to reform the formed ethylene faster than its polymerisation at high temperature. By contrast, polymerisation kinetics becomes competitive with ethylene reforming at 500 °C.

3.3.4. Catalyst NiSiF

As for the FP-prepared samples, sample NiSiF showed very stable and satisfactorily performing when tested at 750 °C. In analogy with NiSiL, we observed a very low conversion of water. This parameter seems tightly bound to the support nature, being indeed similar also for both the zirconia supported samples, irrespectively from the preparation procedure. By keeping constant the support, water conversion is of course increasing with higher activity for the WGS reaction (lower CO/CO_2 ratio) and it may have a close relationship with the overall trend of the C balance during the whole test (coke gasification). However, water conversion showed to increase when passing from silica to zirconia.

The test at 625 °C was also satisfactory, leading to 100% carbon balance, total conversion of ethanol without any by-product and to an optimal hydrogen productivity. By contrast, when decreasing the reaction temperature to 500 °C the sample was not very stable initially. The average C balance under regime conditions was among the best ones at the lowest testing temperature, overcoming by almost 15 points% that of sample NiSiL. However, this parameter monotonously increased from ca. 77 to ca. 91% (Fig. 14), while ethanol conversion started decreasing after 1 h-on-stream from 100 to ca. 80% (at 4 h-on-stream), kept stable until the end of the test, at difference with samples prepared by impregnation which maintained a full conversion for the whole run. The selectivity to methane was constantly nil, but that of acetaldehyde progressively increased with decreasing conversion, up to 7.7%.

3.3.5. Catalyst NiZrF

Finally, NiZrF led to full ethanol conversion at both 750 and 625 °C, without by-products and optimal C balance. Unfortunately, the H_2 productivity was a bit lower than expected due to insufficient promotion of the WGS reaction, i.e. high CO/CO_2 ratio, as observed also for sample NiZrL.
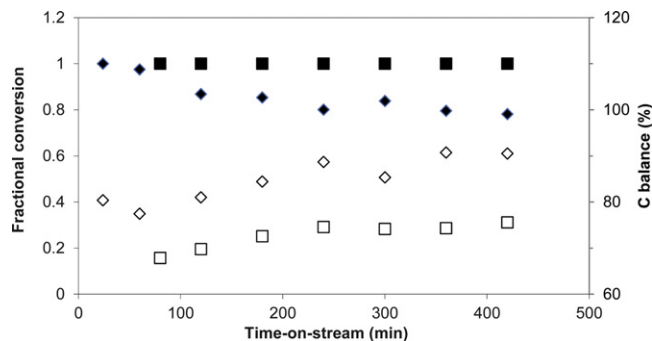
The most interesting considerations for this sample hold for the test at 500 °C (Fig. 15). Indeed, ethanol conversion was poor and the selectivity to by-products relatively high ($S_{CH_4} = 8.0\%$ and $S_{CH_3CHO} = 8.5\%$), but the C balance was significantly higher than for every other sample tested under the same conditions. This parameter was even higher than what obtained during the blank test at 500 °C, since only a portion of the reactor was fully exposed to the reactants feed. Indeed, when recovering the quartz beads after the blank test all the filling material was dirty, whereas during common activity testing at 500 °C only the portion located before the catalytic bed showed coke accumulation.

More precisely, ethanol conversion was complete at the beginning of the test, with low C balance, as depicted in Fig. 12. One may also notice that ethylene selectivity was nil at the beginning of the test, but it progressively increased together with acetaldehyde (Fig. 15).

Hence, one may conclude that ethanol dehydration and polymerisation occurred over the active sites deactivating them. The catalyst performed stably since then, but its activity was insufficient to reform completely methane, as observed also for the other ZrO_2-supported sample. After deactivation occurred also ethanol, acetaldehyde and ethylene were incompletely reformed. Though catalytic activity was not optimal, the satisfactory C balance of NiZrF at the lowest operating temperature opens the way to the possible modulation of the reaction conditions to improve conversion and selectivity. Indeed, while activity is the key for samples comparison on the lab scale, in order to develop industrially viable catalysts, durability is a primary parameter, followed by selectivity and activity. If extensive coking occurs, even if not affecting conversion in the time scale of the present tests, unacceptable waste of reagents occurs, as well as possible deactivation during prolonged use. On the contrary, activity may be increased by tuning other operating parameters, i.e. contact time.
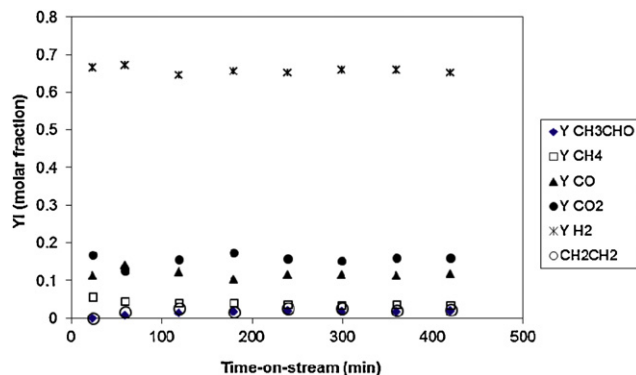

Fig. 15. Products distribution during activity testing of sample NiZrF. Reaction temperature 500 °C.

3.3.6. General comments

All the catalysts performed satisfactorily when tested at 625 and 750 °C. Full ethanol conversion was reached without any gaseous by-product and the C balance was always 100% except for the NiZrL sample when tested at 625 °C. The best results were achieved with NiSiF at 625 °C due to the highest H_2 productivity coupled with 100% C balance and low CO/CO_2 ratio.

Differences among these catalysts became more evident when tested at 500 °C, though not optimal catalyst formulation was found yet among these samples to operate at such temperature. For example, the silica-supported samples were active also for methane reforming even at such low temperature, while selectivity to methane was not nil when using zirconia as support. Silica also promoted more efficiently the WGS reaction at every temperature, so decreasing the CO/CO_2 ratio. High H_2 productivity was achieved with NiSiL and NiZrL, though accompanied by poor C balance, the opposite holding for the FP-prepared samples. Nevertheless, it would be interesting to operate at low temperature, thus some comments are reported in the following to understand the reasons of catalyst failure at 500 °C.

Coking became significant at 500 °C, as predicted by thermodynamic reasons, and it may be correlated with Ni particle size. It is indeed known from the literature that smaller Ni particles are less prone to coking than bigger ones in the reforming of CH_4. The reason of such behaviour should be searched in the mechanism of coke formation over Ni [54–56]. The growth of carbon nanofibers in such case involves methane adsorption on the surface and its conversion into adsorbed carbon [57]. Then, carbon segregates into the layers near the surface by diffusion through Ni and precipitation on the rear side of the Ni crystal. Small Ni crystal size results in a large saturation concentration leading to a low driving force of carbon diffusion and hence a lower coking rate.

The interaction between Ni and the support influences this mechanism as well. Supports characterised by high oxygen mobility, such as ZrO_2 or CeO_2, are able to oxidise carbon [54]. Additionally, basic supports such as MgO and CaO can favour coke gasification [58]. However, they also affect the electronic properties of the supported Ni particles, and hence their reactivity with carbon, thus influencing the rate of coking.

From the point of view of resistance to coking, ZrO_2 showed a good support, since both the FP-prepared samples were characterised by higher C balance at 500 °C and the latter was systematically higher for the ZrO_2-supported samples than for the SiO_2-based ones. Coking exhibited a dependence on Ni particle size, since the lower was the latter parameter (Table 1) the lower was coke deposition at 500 °C (Table 3). Therefore, a strong metal support interaction, evidenced by harder reducibility allowed to keep Ni well dispersed, thus depressing coking. Unfortunately, the most active sites for C nucleation are the same which lead to the activation of the substrate [59]. Therefore, if C diffusion towards the rear of the Ni particle is progressively inhibited, but coke is not efficiently removed, the partial blockage of the active site may occur leading to lower catalytic activity, as likely occurred in the case of NiZrF.

Coking could be also interpreted on the basis of catalyst acidity. Coke deposition may take place on the support only, or at the interface between the metal and the support, so unaffecting of catalyst activity during time-on-stream. For instance, only silanols were observed for NiSiL, while NiSiF was characterised by the presence of silanols and by some Lewis acid sites attributed to Ni. Silanols may be connected with coke deposition, evidenced by a low C balance at reactor outlet. However, sample NiSiL showed a stable behaviour for the whole duration of the test (8 h), without any acetaldehyde formation, though characterised by unacceptable carbon loss when tested at 500 °C. On the contrary, sample NiSiF showed 100% conversion with very low C balance at the beginning of the test under the same conditions. This likely corresponded to coking of the Ni active sites showing stronger Lewis acidity with a decrease of catalytic activity until their complete deactivation. After this first time lapse, catalyst performance returned stable, but characterised by 80% ethanol conversion, only.

It should be noticed that such deactivation was reversible, *i.e.* the original catalytic activity was attained when heating at 625 °C. Therefore we believe that significant metal sintering may be ruled out to explain the observed activity loss. More likely, coking of active sites may have occurred, so that, when increasing back the reaction temperature to 625 °C, coke gasification took place and optimal activity was again achieved.

Coke deposition over the support does not influence ethanol conversion or the reforming activity for acetaldehyde. However, a poorer water activation may occur, ending in decreasing activity for WGS. This was noticed for sample NiSiL, which showed very stable reforming performance. However, coking likely occurring on the support surface led to increasing CO selectivity with time-on-stream (Fig. 13).

Medium Lewis acidity due to Zr(IV) surface sites seems less critical, carbon balance being always higher than for the silica supported samples as already mentioned.

4. Conclusions

Silica and zirconia supported catalysts were prepared by different methods, inducing variable specific surface area, metal dispersion and metal/support interaction. All the samples were tested under different conditions for the steam reforming of ethanol. At 625 and 750 °C good catalytic performance was achieved by every sample. The best results were obtained with NiSiF, prepared by FP, when tested at 625 °C, leading to the highest H_2 productivity, to the lowest CO/CO_2 ratio and to 100% carbon balance without by-products in the outflowing gas.

Significant differences between the prepared catalysts appeared during testing at 500 °C, though not optimal catalyst formulation was found yet among these samples to operate at such temperature. Indeed, high H_2 productivity was achieved with NiSiL and NiZrL, though accompanied by poor C balance and *vice versa* for the FP-prepared catalysts.

Coking led to significantly low C balance when Ni particle size was bigger. Satisfactory C balance was observed when high dispersion was achieved, though unfortunately accompanied by very poor conversion and hydrogen productivity. Both silanols and Lewis Zr(IV) acid sites were associated to coke deposition on the support surface, though this was not correlated to a decrease of catalytic activity for reforming, but in case only to some decrease of WGS activity due to poor water activation on support surface. Of course the drawback was significant carbon loss, especially for sample NiSiL. By contrast, when Lewis acidity was due to Ni sites, catalyst deactivation may become evident, with a progressive decrease of ethanol conversion and increasing selectivity to acetaldehyde.

Metal support interaction also showed very important to determine both catalytic activity and thermal stability of the catalyst. A lower metal reducibility was correlated to a higher metal–support interaction, which stabilises Ni in a more dispersed form. This led to much lower coking during testing at 500 °C.

References

[1] G.A. Deluga, J.R. Salge, L.D. Schmidt, X.E. Verykios, Science 303 (2004) 993.
[2] D.K. Liguras, D.I. Kondarides, X.E. Verykios, Appl. Catal. A: Gen. 43 (2003) 345.
[3] A.N. Fatsikostas, D.I. Kondarides, X.E. Verykios, Catal. Today 75 (2002) 145.
[4] A.N. Fatsikostas, X.E. Verykios, J. Catal. 225 (2004) 439.
[5] A.C. Basagiannis, X.E. Verykios, Appl. Catal. A: Gen. 308 (2006) 182.
[6] V.A. Kirillov, V.D. Meshcheryakov, V.A. Sobyanin, V.D. Belyaev, YuI. Amosov, N.A. Kuzin, A.S. Bobrin, Theor. Found. Chem. Eng. 42 (2008) 1.
[7] M. Benito, R. Padilla, A. Serrano-Lotina, L. Rodríguez, J.J. Brey, L. Daza, J. Power Sources 192 (2009) 158.
[8] L.J.I. Coleman, W. Epling, R.R. Hudgins, E. Croiset, Appl. Catal. A: Gen. 363 (2009) 52.
[9] A.J. Vizcaíno, A. Carrero, J.A. Calles, Int. J. Hydrogen Energy 32 (2007) 1450.
[10] J. Xuan, M.K.H. Leung, D.Y.C. Leung, M. Ni, Renew. Sust. Energy Rev. 13 (2009) 1301.
[11] S.Q. Chen, Y. Liu, Int. J. Hydrogen Energy 34 (2009) 4735.
[12] F. Frusteri, S. Freni, V. Chiodo, L. Spadaro, G. Bonura, S. Cavallaro, J. Power Sources 132 (2004) 139.
[13] S. Freni, S. Cavallaro, N. Mondello, L. Spadaro, F. Frusteri, J. Power Sources 108 (2002) 53.
[14] M. Ni, D. Leung, M. Leung, Int. J. Hydrogen Energy 32 (2007) 3238.
[15] A.J. Vizcaíno, A. Carrero, J.A. Calles, Catal. Today 146 (2009) 63.
[16] D.L. Trimm, Catal. Today 37 (1997) 233.
[17] H.W. Chen, C.Y. Wang, L.T. Tseng, P.H. Liao, Catal. Today 97 (2004) 173.
[18] G. Busca, T. Montanari, C. Resini, G. Ramis, U. Costantino, Catal. Today 143 (2009) 2.
[19] A. Lima da Silva, C. de Fraga Malfatti, I.L. Müller, Int. J. Hydrogen Energy 34 (2009) 4321.
[20] G.L. Chiarello, I. Rossetti, L. Forni, P. Lopinto, G. Migliavacca, Appl. Catal. B: Environ. 72 (2007) 218.
[21] G.L. Chiarello, I. Rossetti, L. Forni, P. Lopinto, G. Migliavacca, Appl. Catal. B: Environ. 72 (2007) 227.
[22] E. Ghedini, M. Signoretto, F. Pinna, G. Cruciani, Catal. Lett. 125 (2008) 359.
[23] F. Zane, S. Melada, M. Signoretto, F. Pinna, Appl. Catal. A: Gen. 299 (2006) 137.
[24] V. Nichele, M. Signoretto, F. Menegazzo, A. Gallo, V. Dal Santo, G. Cruciani, G. Cerrato, Appl. Catal. B: Environ. 111–112 (2012) 225–232.
[25] G.L. Chiarello, I. Rossetti, L. Forni, J. Catal. 236 (2005) 251.
[26] G.L. Chiarello, I. Rossetti, P. Lopinto, G. Migliavacca, L. Forni, Catal. Today 117 (2006) 549.
[27] Selected Powder Diffraction Data, vol. 1–40, Miner. DBM, JCPDS, Swarthmore, PA, 1974–1992.
[28] S. Brunauer, P.H. Emmett, E. Teller, J. Am. Chem. Soc. 60 (1938) 309–319.
[29] E.P. Barrett, L.G. Joyner, P.P. Halenda, J. Am. Chem. Soc. 73 (1951) 373–380.
[30] L. Fabbrini, A. Kryukov, S. Cappelli, G.L. Chiarello, I. Rossetti, C. Oliva, L. Forni, J. Catal. 232 (2) (2005) 247, Impact factor: 4.533, Times cited: 12.
[31] I. Rossetti, L. Fabbrini, N. Ballarini, C. Oliva, F. Cavani, A. Cericola, B. Bonelli, M. Piumetti, E. Garrone, H. Dyrbeck, E.A. Blekkan, L. Forni, J. Catal. 256 (2008) 45.
[32] I. Rossetti, L. Fabbrini, N. Ballarini, C. Oliva, F. Cavani, A. Cericola, B. Bonelli, M. Piumetti, E. Garrone, H. Dyrbeck, E.A. Blekkan, L. Forni, Catal. Today 141 (2009) 271.
[33] C. Oliva, S. Cappelli, I. Rossetti, N. Ballarini, F. Cavani, L. Forni, Chem. Eng. J. 154 (2009) 131.
[34] B. Huang, X. Li, S. Ji, B. Lang, F. Habimana, C. Li, J. Nat. Gas Chem. 17 (2008) 225–231.
[35] Y.Q. Song, D.H. He, B.Q. Xu, Appl. Catal. A: Gen. 337 (2008) 19.
[36] M. Lindo, A.J. Vizcaino, J.A. Calles, A. Carrero, Int. J. Hydrogen Energy 35 (2010) 5895.
[37] S. He, Q. Jing, W. Yu, L. Mo, H. Lou, X. Zheng, Catal. Today 148 (2009) 130.
[38] B. Pawelec, S. Damyanova, K. Arishtirova, J.L.G. Fierro, L. Petrov, Appl. Catal. A: Gen. 323 (2007) 188.
[39] V. García, J.J. Fernández, W. Ruíz, F. Mondragón, A. Moreno, Catal. Commun. 11 (2009) 240.
[40] G. Busca, C. Resini, in: R.A. Meyers (Ed.), Encyclopedia of Analytical Chemistry, Wiley and Sons Ltd., Chichester, 2000, p. 10984.
[41] L. Kubelková, J. Nováková, N.I. Jaeger, G. Schulz-Ekloff, Appl. Catal. A: Gen. 95 (1993) 87.
[42] S. Derrouiche, D. Bianchi, Appl. Catal. A: Gen. 313 (2006) 208.
[43] V. Sanchez Escribano, M.A. Larrubia Vargas, E. Finocchio, G. Busca, Appl. Catal. A: Gen. 316 (2007) 68–74.
[44] M.A. Vannice, in: J.R. Andeson, M. Boudart (Eds.), Catalysis, Science and Technology, vol. 3, Springer Verlag, 1982, p. 139.
[45] C. Resini, T. Venkov, K. Hadjiivanov, S. Presto, P. Riani, R. Marazza, G. Ramis, G. Busca, Appl. Catal. A: Gen. 353 (2009) 137.
[46] M. Garcia Dieguez, E. Finocchio, M.Á. Larrubia, L.J. Alemany, G. Busca, J. Catal. 274 (2010) 11.
[47] L. Barattini, G. Ramis, C. Resini, G. Busca, M. Sisani, U. Costantino, Chem. Eng. J. 153 (2009) 43.
[48] F. Díaz Alvarado, F. Gracia, Chem. Eng. J. 165 (2010) 649.
[49] J.D.A. Bellido, E.M. Assaf, J. Power Sources 177 (2008) 24.
[50] X. Deng, J. Sun, S. Yu, J. Xi, W. Zhu, X. Qiu, Int. J. Hydrogen Energy 33 (2008) 1008.
[51] J. Bussi, N. Bespalko, S. Veiga, A. Amaya, R. Faccio, M.C. Abello, Catal. Commun. 10 (2008) 33.
[52] A. Denis, W. Grzegorczyk, W. Gac, A. Machocki, Catal. Today 137 (2008) 453.
[53] A. Le Valant, A. Garron, N. Bion, D. Duprez, F. Epron, Int. J. Hydrogen Energy 36 (2011) 311.
[54] G. Centi, S. Perathoner, Catal. Today 148 (2009) 191.
[55] V.M. Gonzalez-Dela Cruz, J.P. Holgado, R. Pereniguez, A. Caballero, J. Catal. 257 (2008) 307.
[56] K.O. Christensen, D. Chen, R. Lødeng, A. Holmen, Appl. Catal. A: Gen. 314 (2006) 9.
[57] D. Chen, K.O. Christensen, E. Ochoa-Fernandez, Z. Yu, B. Tøtdal, N. Latorre, A. Monzòn, A. Holmen, J. Catal. 229 (2005) 82.
[58] T. Horiuchi, K. Sakuma, T. Fukui, Y. Kubo, T. Osaki, T. Mori, Appl. Catal. 144 (1996) 111.
[59] X. Zhang, H. Shi, B.Q. Xu, Angew. Chem. Int. Ed. 44 (2005) 7132.